PAPER

Check for updates

Aqueous colloidal systems of bovine serum albumin and functionalized surface active ionic liquids for material transport†

Gagandeep Singh,[a] Manvir Kaur,[a] Vinod Kumar Aswal[b] and Tejwant Singh Kang [iD] *[a]

Detailed physicochemical and computational investigation are made to explore different aspects of complexation between bovine serum albumin (BSA) and three structurally different surface active ionic liquids (SAILs), 1-dodecyl-3-methylimidazolium chloride, $[C_{12}mim][Cl]$; 3-(2-(dodecylamino)-2-oxoethyl)-1-methyl-1H-imidazol-3-ium chloride, $[C_{12}Amim][Cl]$ and 3-methyl-1-dodecyloxy carbonyl methylimidazolium chloride, $[C_{12}Emim][Cl]$. The interfacial and bulk complexation behavior has been monitored using tensiometry, conductivity, steady-state fluorescence and turbidity measurements. Thermodynamic insights about complexation have been obtained using isothermal titration calorimetry (ITC) measurements whereas molecular docking studies were used to predict the possible binding sites of SAILs on BSA. The information obtained from these studies helped in establishing the formed BSA–SAIL complex as a pH dependent colloidal transport system for controlled transport of a lipophilic dye, Rhodamine 6G (R6G), in aqueous phase, which is supported by confocal laser scanning microscopy (CLSM). In the present work, the effect of functionalization over the alkyl chain of SAILs, modulating the colloidal properties of SAIL–BSA systems, has been explored along with the utilization of these complexes as a pH dependent reversible carrier of lipophilic molecules. It is expected that besides providing basic understanding of colloidal complexes of BSA with SAILs, the present work is expected to be helpful in extending the applications of such colloidal systems for material transport.

1. Introduction

Serum albumins are the most utilized proteins due to their relatively large abundance, ease of purification and multifaceted properties.[1–3] Bovine serum albumin (BSA), is 77% identical and 87% homologous with human serum albumin (HSA),[4,5] which makes it the most versatile model protein for different investigations. BSA is a globular protein having 583 amino acid residues with a molecular mass of 66.3 kDa, which functions as a chief transporter and distributor of various endogenous and exogenous ligand metabolites.[4,6] The molecular structure of native BSA consists of three domains (domain I, II and III, Scheme 1), which are further divided into six sub-domains, two sub-domains for each domain. The globular structure of BSA possess 56% α-helical and 11% β-sheet content.[7,8] BSA can reversibly adopt various spatial conformations at different pH values such as N-isoform at pH 7.4 (heart-like shape), F-isoform at pH 3.5 (cigar-like shape) and E-isoform

at pH 2.7 (denatured form).[9,10] The exceptional stability among other proteins such as long shelf-life (about 19 days), stability towards high temperature (at 60 °C up to 10 hours) and in a wide pH range (pH 4 to 9) along with reversible binding ability towards a variety of bioactive molecules and active pharmaceutical ingredients (APIs) make BSA a robust and imperative protein for physiological investigations.[4,11–13]

The use of surfactants in conjunction with proteins generally gives rise to improved physicochemical properties and functions of proteins.[14,15] This renders the investigations on protein–surfactant interactions very important and therefore a large amount of work has been published in this regard.[16–31] In last decade, a new class of surfactants called as surface active ionic liquids (SAILs) has gained great curiosity from the scientific community owing to their better colloidal and surface active properties as compared to conventional surfactants.[32–45] The inherent amphiphilicity and tailorable properties of SAILs offers a precise control over the hydrophilicity/hydrophobicity of SAILs, required to control their colloidal behavior. The choice of cation and anion along with the possibility of functionalization over head group and alkyl chain adds to their applicability. Therefore, the properties of SAILs could offer more potential futuristic prospects for protein–surfactant applications as compared to conventional ionic surfactants. Till date, very limited reports on SAIL–protein colloidal systems are

[a]*Department of Chemistry, UGC-Centre for Advance Studies – II, Guru Nanak Dev University, Amritsar, 143005, India. E-mail: tejwant.chem@gndu.ac.in; tejwantsinghkang@gmail.com; Tel: +91-183-2258802 ext. 3291*

[b]*Solid State Physics Division, Bhabha Atomic Research Centre, Mumbai 400085, India*
† Electronic supplementary information (ESI) available. See DOI: 10.1039/c9ra05549e
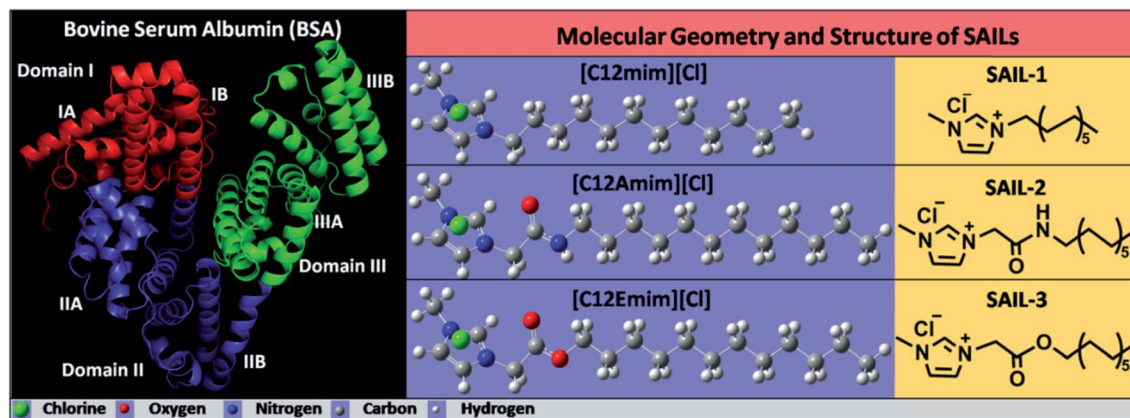
Scheme 1 Molecular geometry and structure of BSA (left) and SAILs (right) used in present study.

available.[8,46–57] Different proteins such as BSA, Gelatin and β-lactoglobulin (β-LG) has been investigated for their complexation with SAILs, where the length of alkyl chain and nature of head group of SAIL has been found to exert significant influence on complexation behavior of BSA with SAILs.[8,46–49,56,57] It is stressed that in most of the investigations, SAILs without any functionalization of ionic head group or alkyl chain have been employed with the exception of few studies.[8,46,48] A contrasting complexation behavior of functionalized SAILs as compared to non-functionalized ones towards BSA,[8] Gelatin[48] and β-lactoglobulin (β-LG)[46] has been observed. Different types of SAIL–protein complexes varying in morphology, internal structure and hydrophobicity *etc.*, governed by the nature and extent of varying set of interactions has been observed. It has been found that both the nature of protein and functionalization of alkyl chain of SAIL affect the complexation phenomenon. This along with the formation of unique self-assembled structures of BSA and functionalized SAILs,[8] previously reported by our group prompted us to further extent the study to explore physico-chemical aspects of such complexation, in detail. In past, no attempt has been made to identify the binding location of SAILs on BSA, which certainly would assist in understanding the nature of interactions at molecular level. Moreover, such BSA–SAIL complexes, owing to lack of structural functionality, has not been investigated for any potential application in past. Therefore, relying on the changes in pH dependent conformations of BSA and interactions between SAILs and BSA, we have also investigated the formed SAIL–BSA colloidal complexes as potential carriers of lipophilic molecules.

Herein, we have carried out detailed physicochemical studies on complexation behavior of BSA with three structurally different SAILs: 1-dodecyl-3-methylimidazolium chloride, [C_{12}mim][Cl]; 3-(2-(dodecylamino)-2-oxoethyl)-1-methyl-1*H*-imidazol-3-ium chloride, [C_{12}Amim][Cl] and 3-methyl-1-dodecyloxy carbonyl methylimidazolium chloride, [C_{12}Emim] [Cl]. A multi-technique approach is employed to explore the interfacial as well as bulk behavior of BSA–SAIL colloidal systems. Computed simulation (AutoDock Vina) has been used to further probe the binding site of SAILs on BSA. The knowledge gained from various physico-chemical studies has been

used to establish the applicability of formed BSA–SAIL-2 colloidal complex (as a representative) as pH dependent transporter of a lipophilic dye, Rhodamine 6G (R6G), reversibly, which has been supported by confocal laser scanning microscopy (CLSM) studies. The interferences gained from different techniques has been corroborated and compared with the literature reports wherever possible. The present work highlight the dynamics of protein–SAILs interactions and is expected to help in establishing a new platform for encapsulating lipophilic drugs in protein–SAIL based colloidal complexes in aqueous medium.

2. Materials and methods

The interfacial and bulk complexation behavior of SAILs with BSA (Scheme 1) was investigated using titration method. Aqueous concentrated stock solutions of investigated SAILs were added to aqueous solution containing 0.1% BSA (w/v) in standard phosphate buffer solution (PBS, pH = 7.2, I = 5 mmol L^{-1}) and the observations were made using various state of art techniques. The concentration of BSA employed (0.1%) is chosen, as one where maximum extent of interactions between BSA and SAILs has been observed without aggregation of BSA, based on fluorescence measurements performed at fixed concentrations (one above and one below to critical micelle concentration) of SAILs by varying the concentration of BSA (Fig. S1, ESI†). The detailed information about the experimental setup is, provided in Annexure S1, ESI.†

3. Results and discussion

3.1. Interfacial behavior of SAIL–BSA colloidal systems

The comparative plots of tensiometric profiles of investigated SAILs in the presence and the absence of 0.1% BSA, in aqueous buffer solutions, are shown in Fig. 1A–C. The lower value of surface tension ($\gamma \approx 54$ mN m^{-1}) in aqueous solution containing BSA as compared to that without BSA ($\gamma \approx 71$ mN m^{-1}) is ascribed to surface active nature of BSA.[56,57] The difference in nature of surface tension profiles of SAILs, with and without BSA, signifies the presence of interactions between SAILs and BSA. In case of SAIL-1, γ decreases continuously without
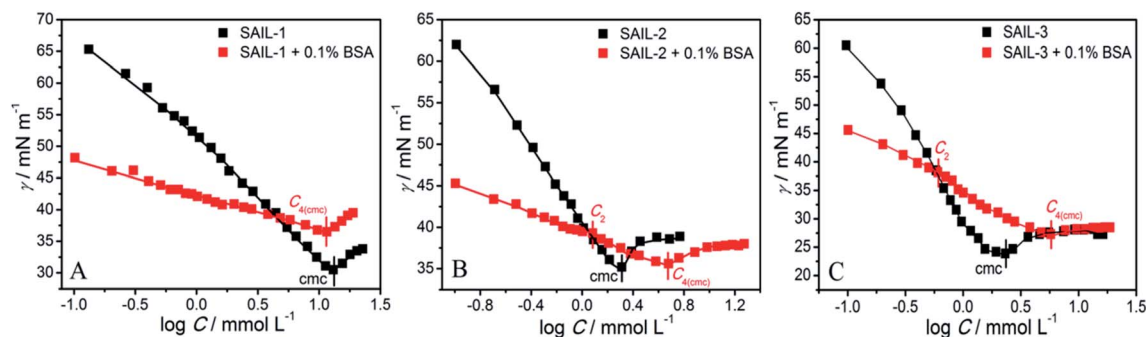
Fig. 1 (A–C) Variation of surface tension in aqueous phosphate buffer solution with and without BSA as a function of concentration of different SAILs at 298.15 K.

showing any significant transition till $C_{4(cmc)}$ similar to that shown by SAIL-1 in the absence of BSA.

A higher value of γ around $C_{4(cmc)}$ suggests the presence of SAIL-1–BSA complex at air–solution interface, which hinders the adsorption of incoming SAIL ions. The monomeric complexation of investigated SAILs, in bulk, has been reported previously resulting in the formation of SAIL–BSA monomer complex (MC) till a concentration, C_1, which even started to self-assemble in very dilute concentration range.[8] Such self assembly of SAIL–BSA MCs becomes relatively more prominent near C_2 which is marked as aggregate complex (AC) stage.[8] However the absence of any break-point corresponding to change in surface behavior indicates that the complexation of SAILs with BSA is a continuous phenomenon. Once formed BSA–SAIL-1 MCs tends to grow in size *via* SAIL mediated self-assembly with increase in concentration of SAIL-1 at air–solution interface. SAIL-2 and SAIL-3 follow contrasting complexation behavior with BSA, as suggested by the presence of different transitions in respective tensiometric profiles, as compared to that observed in case of SAIL-1. There is a weak transition (C_2) in tensiometric profile of SAIL-2 and SAIL-3 in the presence of BSA, where γ decreases with a marginally higher slope beyond C_2 till $C_{4(cmc)}$. This is assigned to partial dissolution of SAIL–BSA complexes into the bulk after C_2 and the occupancy of air–solution interface by respective SAIL ions, which is supported by rise in turbidity in similar concentration regime (discussed later). SAIL-1 interacts with negatively charged[8] BSA (ζ-potential ≈ -18 mV at pH 7.4) *via* electrostatic and hydrophobic interactions whereas SAIL-2 and SAIL-3 offer

additional synergistic H-bonding interactions, which affects the interactional process. It is inferred that SAIL-1–BSA complex (MCs and ACs) remains stable at air–solution interface in the whole concentration range whereas ACs formed by SAIL-2 and SAIL-3 undergo dissolution towards bulk at higher concentration of respective SAILs. This is also justified by the similarity in values of γ at or beyond $C_{4(cmc)}$ in the absence and presence of BSA owing to occupancy of air–solution interface by SAIL molecules.

As can be seen from Tables 1 and S2 (ESI†), critical micelle concentration (cmc) of SAIL-2 and SAIL-3 is found to be higher in presence of BSA as compared to their respective solutions without BSA, where as SAIL-1 exhibit relatively lower cmc in the presence of BSA. The presence of amide and ester-moiety in SAIL-2 and SAIL-3 enables these SAILs to interact synergistically through H-bonding along with other set of interactions with BSA and thus more number of SAIL ions of SAIL-2 and SAIL-3 interacts with BSA[8] as compared to SAIL-1 leading to higher cmc in presence of BSA in case of SAIL-2 and SAIL-3. This is supported by experimental measurements where the number of SAIL ions associated per molecule of BSA is found to be 69, 111 and 210 for SAIL-1, SAIL-2 and SAIL-3, respectively (Table S1, Fig. S2 and S3, ESI†). Further, various interfacial parameters of interest *i.e.* interfacial tension at cmc (γ_{cmc}), the effectiveness of surface tension reduction (π_{cmc}), minimum area per molecule at air–solution interface (A_{min}), Gibbs' surface excess (Γ_{max}), and the standard free energy of adsorption (ΔG°_{ads}), were calculated using surface tension data by employing standard procedures (Annexure S2, ESI†) and are provided in Table S3 (ESI†).

Table 1 Values of concentration corresponding to various transitions, namely, C_1, C_2, C_3, and $C_{4(cmc)}$, obtained during the complexation of SAILs with BSA as obtained from different techniques (surface tension, ST; conductivity, Cond.; pyrene fluorescence, I_1/I_3; isothermal titration calorimetry, ITC; and turbidity, Turb.). All the transitions correspond to concentration in mmol L^{-1}

	SAIL-1				SAIL-2				SAIL-3			
	C_1	C_2	C_3	$C_{4(cmc)}$	C_1	C_2	C_3	$C_{4(cmc)}$	C_1	C_2	C_3	$C_{4(cmc)}$
ST	—	—	—	11.62	—	1.21	—	4.76	—	0.59	—	5.69
Cond.	—	—	—	9.46	0.34	—	—	6.52	0.41	—	—	5.72
I_1/I_3	0.84	—	2.85	3.34	0.35	1.24	2.47	2.95	0.25	0.65	2.46	2.89
ITC	—	3.14	9.14	14.56	—	1.74	3.42	5.03	—	1.74	2.90	4.46
Turb.	1.69	2.54	—	9.09	0.39	0.78	—	2.86	0.45	0.77	—	2.62

The higher values of γ_{cmc} for investigated systems in the presence of BSA as compared to that observed in the absence of BSA is indicative of decreased efficacy of SAILs to populate the air–solution interface in the presence of BSA. A_{min} of SAILs in the presence of BSA is found to be increased by 3.3, 3.7 and 3.3 times for SAIL-1, SAIL-2 and SAIL-3 respectively as compared to BSA free solution indicating relatively loose packing of investigated SAIL at air–solution interface in presence of BSA. However, these results are contrary to the previous reports, where A_{min} decreases for biamphiphilic SAILs (BAILs), [C$_4$mim] [C$_8$OSO$_3$] and [C$_{12}$mim][C$_8$OSO$_3$].[56,57] The additional electrostatic and hydrophobic interactions of amphiphilic anion of the investigated BAILs with BSA could have been resulted in such behavior. Relatively more negative values of ΔG°_{ads} in presence of BSA suggest the greater adsorption efficacy of SAIL–BSA complexes over the micellization in bulk.

3.2. Bulk behavior of SAIL–BSA colloidal systems

3.2.1. Conductivity, turbidity and small angle neutron scattering measurements. Conductivity measurements were performed to investigate the complexation behavior in terms of alternations in ionic environment around BSA as a result of complexation with SAILs. The variation of specific conductance (κ) as function of concentration of SAILs in buffer solution of BSA is shown in Fig. 2A–C.

The concentrations corresponding to different transitions obtained from conductivity measurements are provided in Table 1. In case of SAIL-1, the profile of κ in the presence of BSA almost overlaps with that observed in the absence of BSA and

only one transition corresponding to C$_{4(cmc)}$ is observed. This indicates weaker ionic interactions between SAIL-1 and BSA in the whole concentration range where the micellization of SAIL-1 seems not to be affected by the presence of BSA in terms of ionic environment. In case of SAIL-2 and SAIL-3, two transitions, namely C$_1$ and C$_{4(cmc)}$ are observed. The presence of H-bond acceptor–donor and H-bond acceptor capability of amide and ester groups of SAIL-2 and SAIL-3, respectively, synergistically support already existing electrostatic interactions[8] between these SAILs and BSA. This causes relatively stronger transient localization of ions of SAIL-2 and SAIL-3 near the polypeptide chains of BSA, which results in decreased contribution by these charge carriers per unit area leading to increase in κ with relatively lower slope till C$_1$. In case of SAIL-2, below C$_{4(cmc)}$, κ increases with a lower slope in the presence of BSA, which further overlaps with κ observed in the absence of BSA beyond C$_{4(cmc)}$. The overlap of κ beyond C$_{4(cmc)}$ in the absence and presence of BSA, similar to that observed in case of SAIL-1, suggests the formation of BSA-free micelles. On the other hand, in case of SAIL-3, κ increases with relatively lower slope in whole concentration range in the presence of BSA as compared to BSA free systems. This is indicative of relatively stronger interactions SAIL-3 and BSA and is assigned to relatively flexible nature of ester-moiety, which enables SAIL ions to adopt different spatial orientations to maximize the extent of interactions with BSA. The transition at C$_2$ is not observed from conductivity measurements for all the investigated systems despite the fact that SAIL ions interact with BSA leading to formation of MCs followed by ACs in different concentration
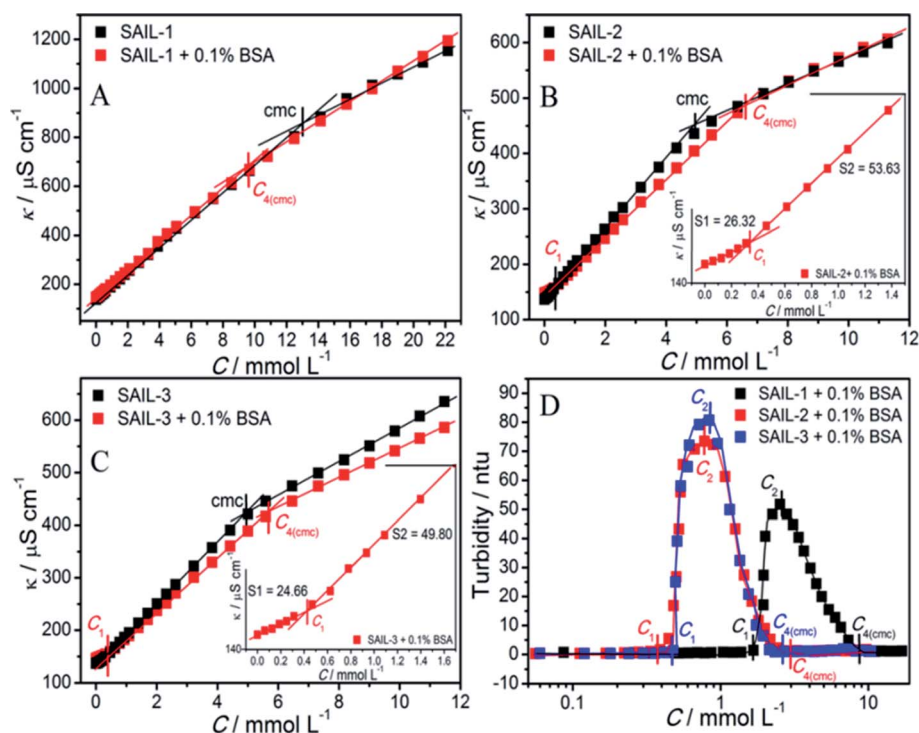

Fig. 2 (A–C) Variation in specific conductivity with and without BSA and (D) turbidity of SAIL–BSA systems, in aqueous phosphate buffer solution as a function of concentration of different SAILs at 298.15 K.
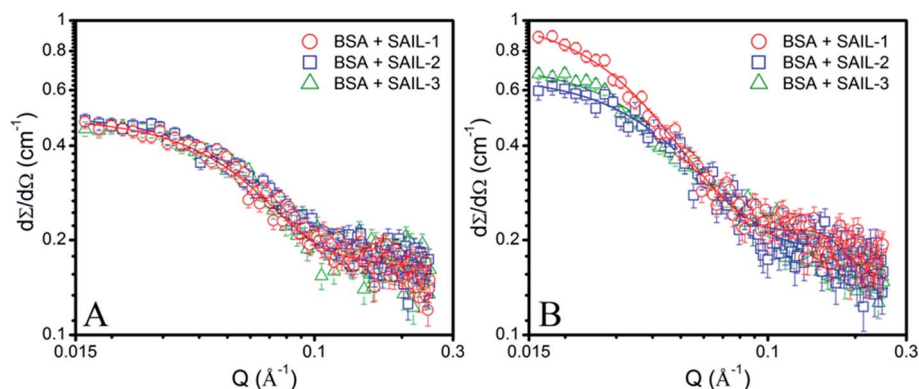
Fig. 3 (A and B) SANS profiles of 1% BSA in presence of different SAIL systems (A) near C_1 and (B) near $C_{4(cmc)}$, along with model fits on obtained data points shown in solid lines.

regimes. This suggests that with increasing concentration of SAILs, after C_1, the hydrophobic interactions begin to gain control over the complexation process, which triggers the self-assembly of SAIL–BSA MCs to ACs near C_2. The substantial contribution of hydrophobic interactions in reorganization of MCs to form ACs could largely render the ionic environment of solution unaffected, which seems to be the reason behind the absence of C_2 and C_3 in the conductivity profile of SAILs. Such observations are quiet common in protein/polymer–SAIL systems.[46,48] Further information about the degree of counter-ion binding (β) and standard free energy of micellization (ΔG°_{mic}) calculated using conductivity measurements (Annexure S2, ESI†) is provided in footnote of Table S3 (ESI†).

Turbidity measurements have been performed to understand the colloidal stability of SAIL–BSA complexes. Till C_1, almost no change in turbidity (Fig. 2D) and DLS[8] profiles of SAILs in BSA solution indicates the formation of very small BSA–SAIL MCs, which don't scatter appreciably and remains well dispersed in solution. This observation is supported by small angle neutron scattering (SANS) measurements (Fig. 3 and Table S4, ESI†). No appreciable change in shape and size of BSA has been observed in the form of BSA–SAIL MCs for all the investigated SAILs. The shape of BSA–SAIL complexes at low SAIL concentration has been found to be oblate-ellipsoid as suggested by SANS measurements, which is similar to that formed by the BSA protein in aqueous medium. Further, the observed size of BSA–SAIL complexes (Table S4A, ESI†) is marginally larger than that observed for BSA (oblate ellipsoid; ε < 1; having semi-major axes 39.7 Å and semi-minor axes 14.6 Å), which is in good agreement with that reported earlier.[58]

However, between C_1 to C_2, turbidity increases abruptly indicating the appearance of large colloidal particles, which gets microscopically phase separated from the solution, in the form of BSA–SAIL ACs formed *via* SAIL mediated self-assembly of BSA–SAIL MCs. Such microscopic phase separation is also supported by the charge neutralization of formed BSA–SAIL MCs.[8] Beyond C_2, the addition of respective SAILs leads to dissolution of formed SAIL–BSA ACs as indicated by sharp decrease in turbidity, which reaches a plateau beyond $C_{4(cmc)}$. Near $C_{4(cmc)}$, BSA gets denatured as also suggested by CD

measurements and the unfolding of BSA exposes the hydrophobic regions towards aqueous environment, which is an entropically unfavorable condition. To counter this change, the BSA gets wrapped around the thus forming micelles of surfactants or SAILs by entrapping water molecules. This leads to the formation of micelle-clusters of BSA–SAIL complexes in the form of necklace-bead like structure.[59,60] The corresponding data obtained by fitting the SANS data using random flight model[31] for oblate-ellipsoidal micelles is provided in Table S4.† It is natural to assume that the electrostatic and hydrophobic interactions between amino acids residues of BSA and SAIL ions at higher SAIL concentration would affect the curvature of forming micelles and this could result in formation of oblate-ellipsoid micelles in comparison to spherical micelles observed in aqueous medium (Fig. S4†). In our previous study, necklace-bead like structures of BSA–SAIL complexes have not been observed[8] from TEM measurements, which is assigned to the fact that such protein–SAIL colloidal systems when dried don't retain their solution phase structure. It is important to mention that no transition corresponding to C_3 has been observed from turbidity measurements contrary to that reported earlier by using DLS measurements.[8] This is due to the fact that different techniques different aspects of complexation.

3.2.2. Spectroscopic investigations. The dynamics of microenvironment of various SAIL–BSA complexes in the investigated concentration range was monitored using pyrene as an external fluorescent molecular probe. The ratio of fluorescence intensity of I_1 (1st vibronic band) to I_3 (3rd vibronic band) is very sensitive towards the polarity of surrounding microenvironment[61] and hence can be used to monitor the polarity changes occurring during the complexation process. Fig. 4A–C shows the variation of I_1/I_3 as a function of concentration of different SAILs in the presence and absence of BSA.

A lower value of I_1/I_3 (1.23) of pyrene in BSA solution as compared to that observed in phosphate buffer (1.71) indicates the adsorption of pyrene in the hydrophobic pockets located on the surface of BSA.[46,56] I_1/I_3 decreases with a relatively lower slope in all of the investigated systems till C_1 indicating a marginal increase in hydrophobicity of forming MCs due to the adsorption of SAIL ions. At C_1, I_1/I_3 value of respective SAIL–
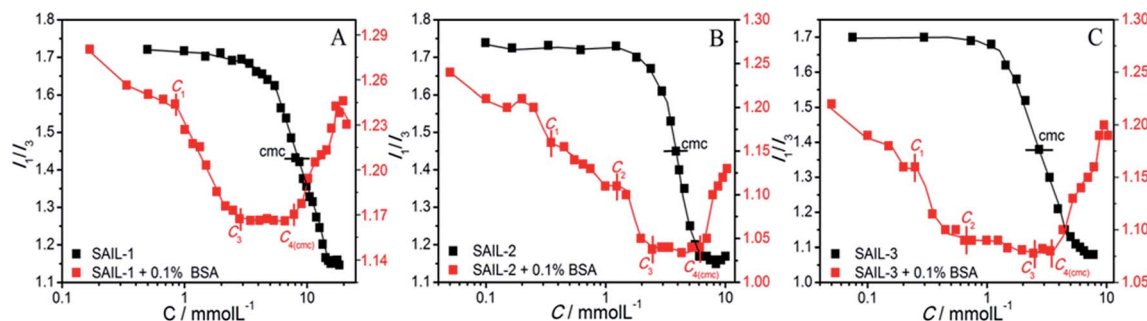
Fig. 4 (A–C) Variation in I_1/I_3 of pyrene in aqueous buffer solution with and without BSA as function of concentration of different SAILs at 298.15 K.

BSA MCs follows the order: SAIL-3 (1.32) < SAIL-2 (1.46) < SAIL-1 (1.56), which indicates the higher hydrophobicity of SAIL-3–MCs complexes. This is in expectation with stronger interactions of H-bonding prone SAIL-2 and SAIL-3 with BSA resulting in the formation of relatively more hydrophobic MCs. After C_1, I_1/I_3 decreases abruptly in all cases till C_3 following different paths. This sharp decrease in I_1/I_3 indicates the lower polarity of ACs formed through self-assembly of MCs mediated *via* hydrophobic interactions offered by SAIL ions[8] in this concentration regime. There is no change in hydrophobicity index of ACs between C_3 and $C_{4(cmc)}$ for all the investigated systems, although in this concentration region, ACs tends to dissolve to form smaller complexes.[8] This suggest negligible change in internal structure of BSA–SAIL complexes in this concentration regime. After $C_{4(cmc)}$, I_1/I_3 begin to rise in all the cases indicating a relative increase in the polarity of SAIL–BSA aggregates. It is quite probable that beyond $C_{4(cmc)}$, the forming micelles containing high surface charge[8,46,48] disintegrate the respective SAIL–BSA ACs into smaller micelle bound/unbound ACs. A similarity in values of I_1/I_3 in the absence and presence of BSA beyond $C_{4(cmc)}$ supports the partition of pyrene into the micelle bound to ACs.

3.2.3. Thermodynamics of complexation between BSA and SAILs. The differential power plots and corresponding enthalpograms, representing the thermodynamic behavior of

investigated SAILs with and without BSA, are provided in Fig. S5A–F and S6A–C, ESI† respectively. To highlight the interactional behavior of SAILs with BSA the difference plot is derived and is provided in Fig. 5.

It is problematic to describe and quantify precisely the types of processes[40,62–65] occurring during complexation, therefore qualitative information has been derived from the obtained thermodynamic data. For all the investigated SAIL–BSA systems, in dilute solution, $\Delta H°$ is endothermic as compared to corresponding aqueous SAILs (Fig. S6A–C, ESI†), where the enthalpic changes are more extensive in case of SAIL-2 and SAIL-3 as compared to SAIL-1. This indicates the significant role of entropic factors associated with the dehydration of SAILs and BSA upon interaction. The breaking of intramolecular H-bonds, specifically in case of SAIL-2 and SAIL-3, results in relatively large endothermic changes. Thereafter, the enthalpic processes favored by attractive H-bonding, electrostatic and hydrophobic interactions between SAIL and BSA compensate the initial entropy factor in the succeeding part of complexation process till $C_{4(cmc)}$. The concentrations corresponding to different transitions obtained from the difference plots (Fig. 5) of enthalpograms corroborate well with other techniques (Table 1). The difference plot of SAILs indicates the dominance of entropic control after $C_{4(cmc)}$ till C_s (C_s, saturation of ITC curve).

For the sake of simplicity, the enthalpy change for interactional process is divided into four parts as C_1–C_2 ($\Delta H_1°$), C_2–C_3 ($\Delta H_2°$), C_3–$C_{4(cmc)}$ ($\Delta H_3°$) and C_4–C_s ($\Delta H_4°$) and the corresponding values of $\Delta H°$ are provided in Table S5 (ESI†). Between C_1 and C_2, exothermic enthalpy change is observed for all of the investigated systems, which is assigned to dominance of electrostatic and hydrophobic interactions in case of SAIL-1, assisted by H-bonding interactions in case of SAIL-2 and SAIL-3. This is justified by the magnitude of $\Delta H_1°$ which follows the order: SAIL-2 (-1.30 kJ mol^{-1}) > SAIL-3 (-0.73 kJ mol^{-1}) > SAIL-1 (-0.46 kJ mol^{-1}). For all the investigated systems, between C_2 to C_3, a slight endothermic rise (entropic process) is observed. Near C_2, the ζ-potential value of BSA–SAIL systems becomes almost zero[8] and remain constant till C_3, indicating the electrostatic saturation of accessible binding sites of BSA. Therefore, such endothermic enthalpy change could be attributed to hydrophobic interactions between the formed complexes and incoming SAIL ions.[8] The values of $\Delta H_2°$ follows the similar
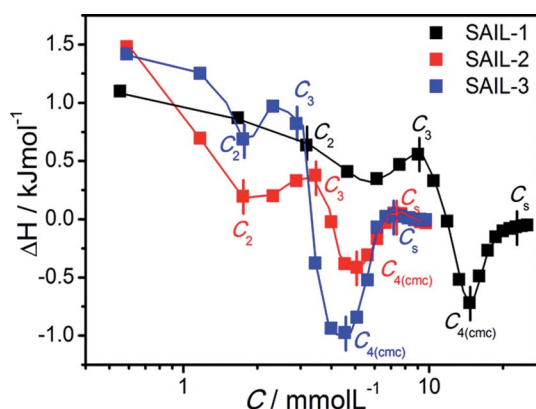

Fig. 5 Difference plot of enthalpograms of SAIL–BSA systems in buffer solution of BSA as the function of concentration of different SAIL at 298.15 K.
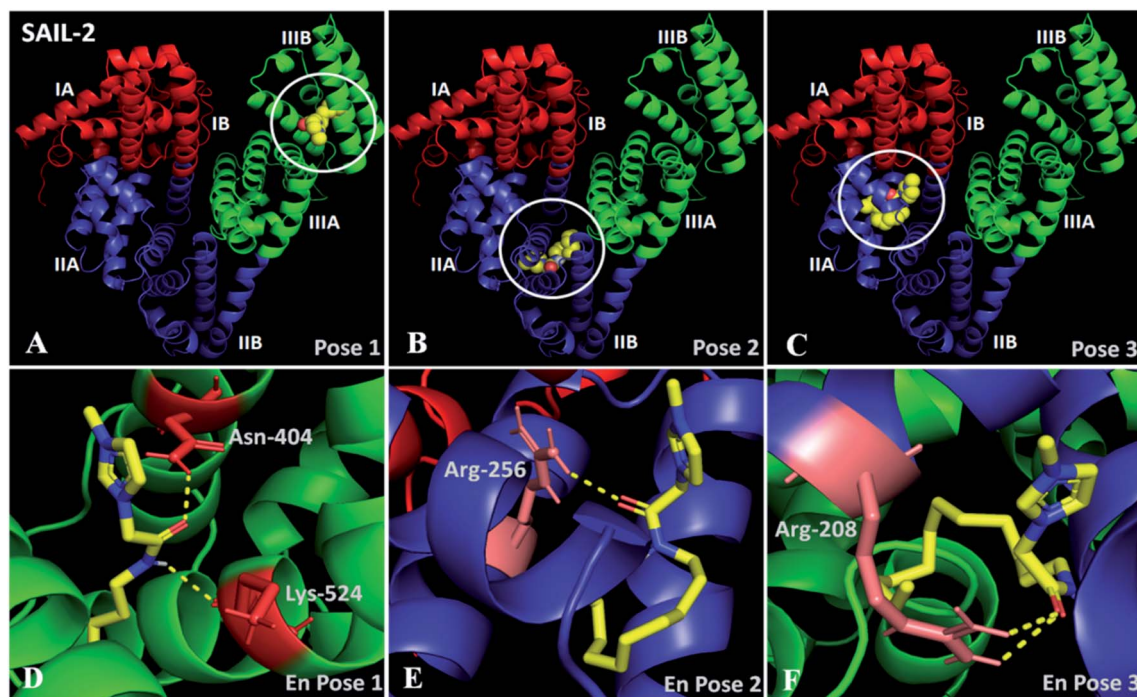
Fig. 6 (A–C) Docked conformation of SAIL-2–BSA system showing the high affinity binding sites for SAIL-2 on BSA in different poses; (D–F) enlarged view of respective poses.

trend as observed for ΔH_1°: SAIL-2 (+0.19 kJ mol^{-1}) > SAIL-3 (+0.14 kJ mol^{-1}) > SAIL-1 (−0.08 kJ mol^{-1}). With further rise in concentration of SAILs, between C_3 and $C_{4(cmc)}$, relatively larger exothermic drop in values of enthalpy change (ΔH_3°) is observed, which for different SAILs, follows the order: SAIL-3 (−1.79 kJ mol^{-1}) > SAIL-1 (−1.28 kJ mol^{-1}) > SAIL-2 (−0.79 kJ mol^{-1}). The order indicates the greater extent of interactions between SAIL-3 and BSA–SAIL-3 ACs between C_3 and $C_{4(cmc)}$, which resulted in the formation of highly ordered self-assembled molecular architecture of SAIL-3–BSA into helical fibers in this concentration regime (at 1.5 mmol L^{-1} of SAIL-3 in 0.1% BSA).[8] Further, the observed endothermic change, after $C_{4(cmc)}$ in all cases, establishes the dominance of entropically favored processes, which is assigned to the dissolution of SAIL–BSA complexes in micellar solution of SAILs.

3.2.4. Molecular docking studies. The preferred binding site of the investigated SAILs on BSA has been determined using molecular docking studies.[66–70] The data obtained from the docking studies reveals that, all the investigated SAILs binds at the high affinity sites of BSA (binding site II and III) however, differ in their mode of interactions with the amino acid residues present in the vicinity of the respective SAILs. This is in line with the literature reports which established the presence of two highly selective and high affinity binding sites for molecules such as fatty acids, tryptophan, octanoate and bilirubin *etc.*, present in sub-domain IIA (site I) and IIIA (site II) (Fig. S7, ESI†) of BSA.[11–13,66] However the mode of binding for two sites is different as site I binds the target ligands *via* hydrophobic interactions whereas site II binds ligands through the combination of H-bonding, electrostatic and hydrophobic

interactions. Besides this, there exist many other low affinity binding sites distributed around various other locations on BSA.[11–13]

In docking studies, nine modes of binding conformations of SAILs are obtained (Table S6, ESI†). The first three poses with high free energy of binding affinities of SAIL-1, SAIL-2 and SAIL-3 towards BSA are shown in Fig. S8 (ESI†), 6A–F and S9 (ESI†), respectively. The investigated SAILs, due to their structural resemblance with hydrophobic moieties like fatty acid and octanoate, bind in domain III as first preference followed by domain II. SAIL-1 being non-functionalized analogue among the investigated SAILs interacts through electrostatic as well as hydrophobic interactions and binds in domain IIIB (Fig. S8A–C†) along with other locations on BSA similar to SAIL-2 and SAIL-3. SAIL-2 (Fig. 6A–F) and SAIL-3 (Fig. S9A–E†), owing to the presence of amide and ester functionality, respectively, forms H-bond acceptor–donor pairs and exhibit various other polar interactions with amino acid residues present at their binding cavity. This corroborates well with the previously made claims that SAIL-2 and SAIL-3 interacts more strongly with BSA as compared to SAIL-1.

In pose 1 (Fig. 6A and D), SAIL-2 is shown to bind in hydrophobic cavity formed between the helices of domain IIB, where it undergoes H-bonding with –NH$_2$ group of Asn-404 and –C═O of Lys-524 through –C═O and –NH moiety, respectively, of amide group of SAIL-2. In pose 2 (Fig. 6B and E), SAIL-2 is shown to bind between the helices of sub-domain IIA and IIB where it forms H-bonding with –NH$_2$ group of Arg-256 through –C═O of amide group. In pose 3 (Fig. 6C and F), SAIL-2 binds in sub-domain IIA, where it makes two polar interactions with –NH$_2$ groups of Arg-208 through its carbonyl group. Similar
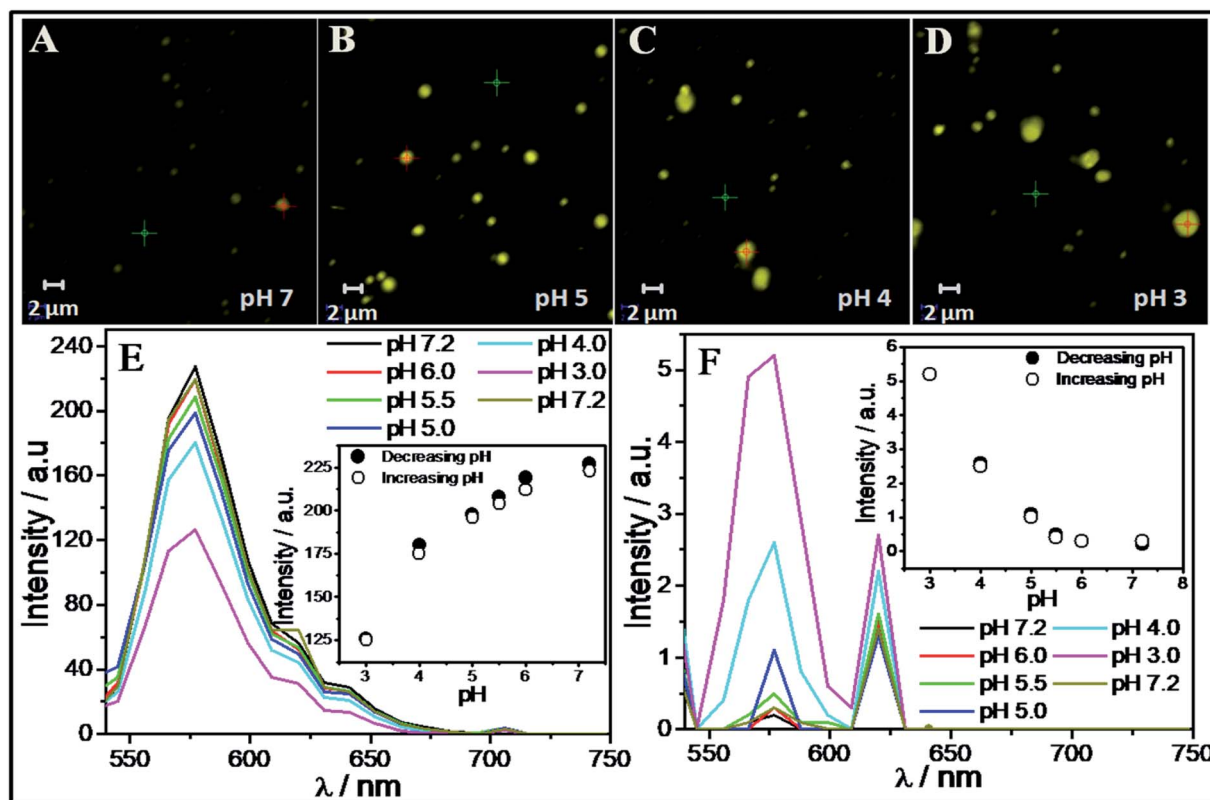
Fig. 7 (A–D) CLSM images of R6G loaded in SAIL-2–BSA aggregates complexes at different pH; (E and F) UV spectra of R6G taken at the colored spots and from background solution as marked in CLSM images.

binding locations have been obtained for SAIL-3, which however differ in their mode of interactions (Fig. S9A–E, ESI†). In pose 1 (Fig. S9A, ESI†), no such polar interactions are observed which is attributed to flexible nature of ester moiety of SAIL-3. The absence of favorable space orientations required for making such polar interactions cannot be ruled out at this stage. In pose 2 (Fig. S9B and D, ESI†), SAIL-3 makes three polar interactions in its binding cavity, one with –NH$_2$ group of Arg-208 via polar oxygen atom of ester linkage and another two between two –NH$_2$ groups of Arg-208 and oxygen atom of carbonyl group. In pose 3 (Fig. S9C and E, ESI†), SAIL-3 makes two polar interactions of oxygen atom of ester linkage with –NH$_2$ group of Arg-198. It is inferred that the investigated SAILs which differ in their molecular structure prefer different binding sites, however the H-bonding prone SAIL-2 and SAIL-3 exhibit similar tendency towards binding in sub-domain IIA with Arg-208.

3.3. Efficacy of BSA–SAIL complexes as colloidal scaffolds for transport

It is inferred that the ACs formed by SAIL-2 and SAIL-3 are relatively more hydrophobic and could show pH dependent structural organization owing to presence of electrostatic interactions between SAILs and BSA. Going with this background, we have investigated pH dependent loading and unloading of a lipophilic dye, Rhodamine 6G (R6G, 25 μM) as a model compound, employing BSA–SAIL-2 colloidal complexes

(0.1%/1 mM, near C$_2$ of SAIL-2) system, as a representative. The entire process has been monitored using CSLM (Fig. 7A–D) equipped with the facility of UV-visible absorption measurements (Fig. 7E and F). The change in absorption intensity corresponding to absorption maxima of R6G ($\lambda_{max} \approx 575$ nm) was monitored both in the colloidal complexes (red-cross, Fig. 7A–D) as well as in bulk (green-cross, Fig. 7A–D) as a function of pH. A decrease in absorption corresponding to λ_{max} of R6G (Fig. 7E) present in BSA–SAIL-2 colloidal complex (red-cross, Fig. 7A–D) with simultaneous increase in absorption of R6G (Fig. 7F) present in bulk solution (green-cross, Fig. 7A–D) with decrease in pH from 7 to 3 indicates the unloading of R6B from BSA–SAIL-2 colloidal complex in solvent rich phase.

Further with increase in pH, the system show reversible uptake of R6G. The pH induced structural changes in investigated BSA–SAIL-2 colloidal complex are supposed to be the reason behind the reversible loading and unloading of R6G. Such changes have been probed by ζ-potential measurements as the alteration in surface charge and size of the ACs was thought to govern the dye loading and delivery. An increase in the values of ζ-potential from −4 mV to 12 mV has been observed while going from pH 7 to 2 (Fig. S10, ESI†). The protonation of negatively charged amino acid residues of BSA, namely Asp, Glu and His at pH 3 and below results in highly positive ζ-potential. Such high extent of protonation could weaken electrostatic interactions between BSA and SAIL-2 in BSA–SAIL-2 colloidal complexes leading to structural

reorganization of complexes. The reversible structural transition from N (pH 7.4) to F-isoform (pH 3.5) with opening up of the inherent globular structure of BSA could diminish the binding site present in the cavity formed by three domains and thus facilitates the release of R6G from its binding site (Fig. S11 and Table S7, ESI†).

The role of increasing hydrophobicity of colloidal complex owing to structural transition from N (pH 7.4) to F isoform (pH 3.5)[10] in release of R6G into the solution along with SAIL ions can't be ruled out as solubility of R6G decreases with decrease in polarity of the solvent.[71] The studies conducted on BSA–SAIL-2 colloidal complex and R6G establishes a new platform for developing new colloidal systems comprising proteins and SAILs (inherently non-toxic) for transport of biologically important lyophobic/lipophilic molecules along with their targeted and controlled release. Further the role of SAILs used in conjunction with proteins for such applications can be easily modified by the choice of anion or cation or by functionalization of SAILs, if needed. Therefore, easily tunable structural and chemical nature of SAIL–protein based scaffold makes such systems as potential candidates for different biomedical applications.

4. Conclusion

The nature of SAILs is found to affect their complexation behavior with BSA. The H-bond acceptor/donor and H-bond acceptor abilities of SAIL-2 and SAIL-3, respectively, produce distinct alternations in the structure of BSA, which resulted in the formation of SAIL–BSA complexes of different shape and morphology at different stages of complexation. The highest surface activity of SAIL-3–BSA complexes at air–solution interface reflects relatively stronger interactions of SAIL-3 with BSA, which modifies the hydrophobic–hydrophilic index of the formed colloidal aggregates at air–solution interface. On the other hand the amide group of SAIL-2 resembles the peptide linkages of protein and stabilizes the polypeptide network at low concentrations. The molecular docking profile of SAIL-2 and SAIL-3 clearly showed the presence of H-bonding and other polar interactions of these SAILs at their binding locations. The studies conducted to understand the physiochemical behavior of SAIL–BSA system inspired us to develop pH dependent reversible carrier of lipophilic molecule such as R6G dye (as a model hydrophobic drug) in SAIL-2–BSA colloidal system, which has been established successfully.

Conflicts of interest

There are no conflicts to declare.

Acknowledgements

References

1 G. J. Quinlan, G. S. Martin and T. W. Evans, *Hepatology*, 2005, **41**, 1211–1219.

2 J. P. Doweiko and D. J. Nompleggi, *JPEN, J. Parenter. Enteral Nutr.*, 1991, **15**, 207–211.

3 M. Roche, P. Rondeau, N. R. Singh, E. Tarnus and E. Bourdon, *FEBS Lett.*, 2008, **582**, 1783–1787.

4 S. Moghaddassi, *Modification of the Bovine Genome for the Large-Scale Production of Human Serum Albumin*, PhD dissertation, Wake Forest University Graduate School of Arts and Sciences, Winston-Salem, North Carolina, December 2013.

5 E. L. Gelamo, C. H. T. P. Silva, H. Imasato and M. Tabak, *Biochim. Biophys. Acta*, 2002, **1594**, 84–99.

6 A. M. Merlot, D. S. Kalinowski and D. R. Richardson, *Front. Physiol.*, 2014, **5**, 299.

7 A. Bujacz, *Acta Crystallogr., Sect. D: Biol. Crystallogr.*, 2012, **68**, 1278–1289.

8 G. Singh and T. S. Kang, *J. Phys. Chem. B*, 2015, **119**, 10573–10585.

9 M. Y. Khan, *Biochem. J.*, 1986, **236**, 307–310.

10 K. Baler, O. A. Martin, M. A. Carignano, G. A. Ameer and J. A. Vila, *J. Phys. Chem. B*, 2014, **118**, 921–930.

11 S. Fujiwara and T. Amisaki, *Biochim. Biophys. Acta*, 2013, **1830**, 5427–5434.

12 U. Kragh-Hansen, *Pharmacol. Rev.*, 1981, **33**, 17–53.

13 J. J. Vallner, *J. Pharm. Sci.*, 1977, **66**, 447–465.

14 C. Pinholt, R. A. Hartvig, N. J. Medlicott and L. Jorgensen, *Expert Opin. Drug Delivery*, 2011, **8**, 949–964.

15 M. C. Manning, J. Liu, T. Li and R. E. Holcomb, *Adv. Protein Chem. Struct. Biol.*, 2018, **112**, 1–59.

16 D. Otzen, *Biochim. Biophys. Acta, Proteins Proteomics*, 2011, **1814**, 562–591.

17 J. Maldonado-Valderrama and J. M. R. Patino, *Curr. Opin. Colloid Interface Sci.*, 2010, **15**, 271–282.

18 T. A. Khan, H.-C. Mahlera and R. S. K. Kishore, *Eur. J. Pharm. Biopharm.*, 2015, **97**, 60–67.

19 A. Chakraborty, D. Seth, P. Setuna and N. Sarkar, *J. Phys. Chem. B*, 2006, **110**, 16607–16617.

20 S. F. Santos, D. Zanetti, H. Fischer and R. Itri, *J. Colloid Interface Sci.*, 2013, **662**, 400–408.

21 S. H. Chen and J. Teixeiria, *Phys. Rev. Lett.*, 1986, **57**, 2583.

22 D. Kelley and D. J. McClements, *Food Hydrocolloids*, 2003, **17**, 73–85.

23 E. L. Gelamo, R. Itri, A. Alonso, J. V. da Silva and M. Tabak, *J. Colloid Interface Sci.*, 2004, **277**, 471–482.

24 T. Chakraborty, I. Chakraborty, S. P. Moulik and S. Ghosh, *Langmuir*, 2009, **25**, 3062–3074.

25 Y. Moriyama, Y. Kawasaka and K. Takeda, *J. Colloid Interface Sci.*, 2003, **257**, 41–46.

26 Y. Li, X. Wang and Y. Wang, *J. Phys. Chem. B*, 2006, **110**, 8499–8505.

27 N. J. Turro, X. G. Lei, K. P. Ananthapadmanabhan and M. Aronson, *Langmuir*, 1995, **11**, 2525–2533.

28 D. Wu, G. Xu, Y. Sun, H. Zhang, H. Mao and Y. Feng, *Biomacromolecules*, 2007, **8**, 708–712.

29 K. P. Ananthapadmanabhan, in *Interactions of Surfactants with Polymers and Proteins*, ed. E. D. Goddard and K. P. Ananthapadmanabhan, CRC Press, Inc, London, UK, 1993, ch. 8.

30 M. N. Jones, *Chem. Soc. Rev.*, 1992, **21**, 127–136.

31 S. Hirlekar, D. Ray, V. K. Aswal, A. Prabhune, A. Nisal and S. Ravindranathan, *Langmuir*, 2019, **35**, 14870–14878.

32 T. Singh, M. Drechsler, A. H. E. Müller, I. Mukhopadhyay and A. Kumar, *Phys. Chem. Chem. Phys.*, 2010, **12**, 11728–11735.

33 Y. Zhao, S. J. Gao, J. J. Wang and J. M. Tang, *J. Phys. Chem. B*, 2008, **112**, 2031–2039.

34 B. Dong, N. Li, L. Zheng, L. Yu and T. Inoue, *Langmuir*, 2007, **23**, 4178–4182.

35 O. A. El Seoud, P. A. R. Pires, T. Abdel-Moghny and E. L. Bastos, *J. Colloid Interface Sci.*, 2007, **313**, 296–304.

36 P. Brown, C. P. Butts, J. Eastoe, D. Fermin, I. Grillo, H.-C. Lee, D. Parker, D. Plana and R. M. Richardson, *Langmuir*, 2012, **28**, 2502–2509.

37 H. Wang, J. Wang, S. Zhang and X. Xuan, *J. Phys. Chem. B*, 2008, **112**, 16682–16689.

38 C. Jungnickel, J. Łuczak, J. Ranke, J. F. Fernandez, A. Muller and J. Thöming, *Colloids Surf., A*, 2008, **316**, 278–284.

39 R. Dutta, S. Ghosh, P. Banerjee, S. Kundu and N. Sarkar, *J. Colloid Interface Sci.*, 2017, **490**, 762–773.

40 J. Bowers, P. Butts, J. Martin, C. Vergara-Gutierrez and K. Heenan, *Langmuir*, 2004, **20**, 2191–2198.

41 P. Brown, C. Butts, R. Dyer, J. Eastoe, I. Grillo, F. Guittard, S. Rogers and R. Heenan, *Langmuir*, 2011, **27**, 4563–4571.

42 P. Brown, C. P. Butts, J. Eastoe, D. Fermin, I. Grillo, H.-C. Lee, D. Parker, D. Plana and R. M. Richardson, *Langmuir*, 2012, **28**, 2502–2509.

43 N. V. Sastry, N. M. Vaghela and V. K. Aswal, *Fluid Phase Equilib.*, 2012, **327**, 22–29.

44 I. Goodchild, L. Collier, S. L. Millar, I. Prokeš, J. C. D. Lord, C. P. B. Butts, J. Bowers, J. R. P. Webster and R. K. Heenan, *J. Colloid Interface Sci.*, 2007, **307**, 445–468.

45 N. V. Sastry, N. M. Vaghela, P. M. Macwan, S. S. Soni, V. K. Aswal and A. Gibaud, *J. Colloid Interface Sci.*, 2012, **371**, 52–61.

46 G. Singh, G. Singh, S. Kancharla and T. S. Kang, *J. Phys. Chem. B*, 2019, **123**, 2169–2181.

47 S. Chabba, R. Vashishat and R. K. Mahajan, *J. Mol. Liq.*, 2018, **259**, 134–143.

48 G. Singh, G. Singh and T. S. Kang, *Phys. Chem. Chem. Phys.*, 2016, **18**, 25993–26009.

49 T. Singh, S. Boral, H. B. Bohidar and A. Kumar, *J. Phys. Chem. B*, 2010, **114**, 8441–8448.

50 P. Bharmoria, M. J. Mehta, I. Pancha and A. Kumar, *J. Phys. Chem. B*, 2014, **118**, 9890–9899.

51 P. Bharmoria, T. J. Trivedi, A. Pabbathi, A. Samanta and A. Kumar, *Phys. Chem. Chem. Phys.*, 2015, **17**, 10189–10199.

52 H. Yan, J. Wu, G. Dai, A. Zhong, H. Chen, J. Yang and D. Han, *J. Lumin.*, 2012, **132**, 622–628.

53 F. Geng, L. Zheng, J. Liu, L. Yu and C. Tung, *Colloid Polym. Sci.*, 2009, **287**, 1253–1259.

54 M. Kumari, J. K. Maurya, U. K. Singh, A. B. Khan, M. Ali, P. Singh and R. Patel, *Spectrochim. Acta, Part A*, 2014, **124**, 349–356.

55 X. Wang, J. Liu, L. Sun, L. Yu, J. Jiao and R. Wang, *J. Phys. Chem. B*, 2012, **116**, 12479–12488.

56 T. Singh, P. Bharmoria, M. Morikawa, N. Kimizuka and A. Kumar, *J. Phys. Chem. B*, 2012, **116**, 11924–11935.

57 P. Bharmoria, K. S. Rao, T. J. Trivedi and A. Kumar, *J. Phys. Chem. B*, 2014, **118**, 115–124.

58 F. Zhang, F. Roosen-Runge, M. W. A. Skoda, R. M. J. Jacobs, M. Wolf, P. Callow, H. Frielinghaus, V. Pipich, S. Prévostf and F. Schreibera, *Phys. Chem. Chem. Phys.*, 2012, **14**, 2483–2493.

59 S. Chodankar, V. K. Aswal, J. Kohlbrecher, R. Vavrin and A. G. Wagh, *J. Phys.: Condens. Matter*, 2007, **19**, 326102–326113.

60 S. H. Chen and J. Teixeira, *Phys. Rev. Lett.*, 1986, **57**, 2583–2586.

61 K. Kalyanasundaram and J. K. Thomas, *J. Am. Chem. Soc.*, 1977, **99**, 2039–2044.

62 R. Kamboj, P. Bharmoria, V. Chauhan, G. Singh, A. Kumar, S. Singh and T. S. Kang, *Phys. Chem. Chem. Phys.*, 2014, **16**, 26040–26050.

63 K. J. Bijma, B. F. N. Engberts, M. J. Blandamer, P. M. Cullis, P. M. Last, K. D. Irlam and L. G. Soldi, *J. Chem. Soc., Faraday Trans.*, 1997, **93**, 1579–1584.

64 K. Bouchemal, *Drug Discovery Today*, 2008, **13**, 960–972.

65 S. Paula, W. Süs, J. Tuchtenhagen and A. Blume, *J. Phys. Chem.*, 1995, **99**, 11742–11751.

66 H.-H. Cai, X. Zhong, P.-H. Yang, W. Wei, J. Chen and J. Cai, *Colloids Surf., A*, 2010, **372**, 35–40.

67 C. Hetényi and D. V. D. Spoel, *Protein Sci.*, 2002, **11**, 1729–1737.

68 O. Trott and A. J. Olson, *J. Comput. Chem.*, 2010, **31**, 455–461.

69 M. M. Jaghoori, B. Bleijlevens and S. D. Olabarriaga, *J. Comput.-Aided Mol. Des.*, 2016, **30**, 237–249.

70 K. Onodera, K. Satou and H. Hirota, *J. Chem. Inf. Model.*, 2007, **47**, 1609–1618.

71 A. Penzkofer and W. Leupacher, *J. Lumin.*, 1987, **37**, 61–72.